ISTITUTO NAZIONALE FISICA NUCLEARE

INFN/BE - 77/1
10 maggio 1977

U. Abbondanno, F. Demanins, A. Giletti, G. Nardelli and C. Tuniz

PROGRESS REPORT ON THE STUDY OF ^{12}N WITH THE $^{10}B(^{3}He;n)^{12}N$ REACTION

SERVIZIO RIPRODUZIONE DELLA
SEZIONE DI TRIESTE DELL'INFN

PROGRESS REPORT ON THE STUDY OF ^{12}N WITH THE $^{10}B(^{3}He;n)^{12}N$ REACTION

U. Abbondanno, F. Demanins, A. Giletti, C. Tuniz
Istituto di Fisica, Università di Trieste
Istituto Nazionale di Fisica Nucleare, Sezione di Trieste
and
G. Nardelli
Istituto di Fisica, Università di Padova
Istituto Nazionale di Fisica Nucleare, Sezione di Padova

A B S T R A C T

The $^{10}B(^{3}He,n)^{12}N$ reaction has been investigated at ^{3}He energies of 4.7 and 5.5 MeV, by using the pulsed-beam time-of-flight technique, in order to obtain detailed information on the energy level structure of ^{12}N. In the region of the excitation energies up to 5.4 MeV 28 levels have been identified, and their energies and widths are reported. Angular distributions have been obtained for various neutron groups corresponding to the levels of the residual nucleus. A comparison has been made between experimental angular distributions and theoretical curves, calculated by assuming the two-proton stripping process as resulting from an incoherent sum of direct reaction (calculated by means of the Distorted Wave Born Approximation) and compound nucleus reaction (calculated by means of the statistical theory). In this way, spin and parity assignments have been confirmed for the ground state ($J^{\pi} = 1^{+}$), the first-excited state ($E_x = 977 \pm 14$ keV, $J^{\pi} = 2^{+}$) and the second-excited state ($E_x = 1215 \pm 23$ keV, $J^{\pi} = 2^{-}$) of ^{12}N. Relative spectroscopic factors have been also calculated for these levels.

1. - INTRODUCTION

The nucleus ^{12}N belongs to that class of nuclei whose present-day spectroscopic information is incomplete and in disagreement when comparison is made between data obtained in different laboratories. This situation becomes evident comparing the energy level structure of ^{12}N with that of the other components of the T = 1 isobaric triplet, i.e. ^{12}C and ^{12}B.(1)(2) Excitation energy, width, spin and parity of the levels are known with good precision for this last two nuclei, whereas, in the case of ^{12}N, there is an evident disagreement for the assignment of the excitation energies and for the determination of the widths of the levels, not to mention the assignment of spin and parity. Comparing the level density of the components of the isobaric triplet, we get the suspicion that, for several experimental reasons, many levels of ^{12}N have not been observed. There is an original reason that produces this situation: in fact, the reactions leading to ^{12}N (an unstable nucleus that can be studied only as residual nucleus of a nuclear reaction and not with scattering measurements) are (1)(3).

i) $^{10}B(^{3}He;n)^{12}N$ Q = 1.569 MeV

ii) $^{12}C(p;n)^{12}N$ Q = -18.126 MeV

iii) $^{12}C(^{3}He;p)^{12}N$ Q = -17.362 MeV

iv) $^{14}N(\gamma;2n)^{12}N$ Q = -30.621 MeV

v) $^{14}N(p;t)^{12}N$ Q = -22.141 MeV

vi) $^{16}O(^{3}He;^{7}Li)^{12}N$ Q = -22.058 MeV

vii) $^{12}N(\beta^{+})^{12}C$ Q = 17.344 MeV

Using the process vii) it is possible to study only the ground state of ^{12}N, because the positon decay of ^{12}N leads to different levels of ^{12}C. All the other processes, a part the reaction i) are endoergic with high Q-value and therefore they preclude the use of Van de Graaff accelerators. Moreover, the experimental detection and analysis of the particle groups, corresponding to the population of the ^{12}N levels, are complicated by many other reactions different from the one we are studying in the exit channel. There is only one exoergic reaction, the process i), that can be produced even by low energy accelerators. The study of this reaction presents the typical experimental difficulties connected with the high

resolution neutron spectrometry in presence of a strong gamma-background produced by the competitive reaction $^{10}B(^{3}He;\gamma)^{13}N$ (Q = 21.638 MeV) [4] and of a neutron background (originated by the process $^{10}B(^{3}He;n-p)^{11}C$ (Q = 0.973 MeV))[5]. However, several researchers have investigated ^{12}N through the process i) [6][7][8][9][10], just because only with this reaction it is possible to study this nucleus at low energies. In the experimental works of ZAFIRATOS et al.[7], ADAMS et al.[8], BOHNE et al.[9] and FUCHS et al.[10], while there is a reasonable agreement for the excitation energies of the levels, some width determination are quite different. The recent study of MAGUIRE et al.[2] using the reaction iii), has confirmed the data regarding the excitation energies, but it reports widths that differ from the values obtained before. For example, the width of the E_x = 4.150 MeV level is twice as large as reported in previous measurements. This situation could arise from the fact that different reactions may populate different analogues state or, more simply, from the fact that because of the finite resolution of the spectrometers groups of levels very close one to another appear as wide single levels. Moreover, the experimental difficulties are increased by the fact that all the excited states of this nucleus are unbound. For these reasons it has been thought that a high resolution investigation of the reaction i) could be interesting in order to obtain new information on the level structure of ^{12}N from the analysis of the several neutron groups emitted in a wide angular range with respect to the direction of the ^{3}He incident beam.

2. - EXPERIMENTAL SET-UP

The measurements described in this report have performed at the 7 MV Van de Graaff accelerator of the "Laboratorio Nazionale di Legnaro", by using the pulsed-beam time-of-flight technique. Two spectrometers, surrounded by hydrogenate materials and lead, were placed on two arms rotating around an axis coincident with the axis of the target (see Fig. 1). The neutron detectors where liquid scintillators NE213, 2" in diameter and 3" long, coupled to 56 DVP photomultipliers. The measurements were carried out with flight paths (L) of 2 and 4,6 meters. The arms could rotate from 0 to 160 degrees with respect to the ^{3}He accelerator beam. We used one spectrometer in order to obtain spectra at various angles and energies of neutrons.

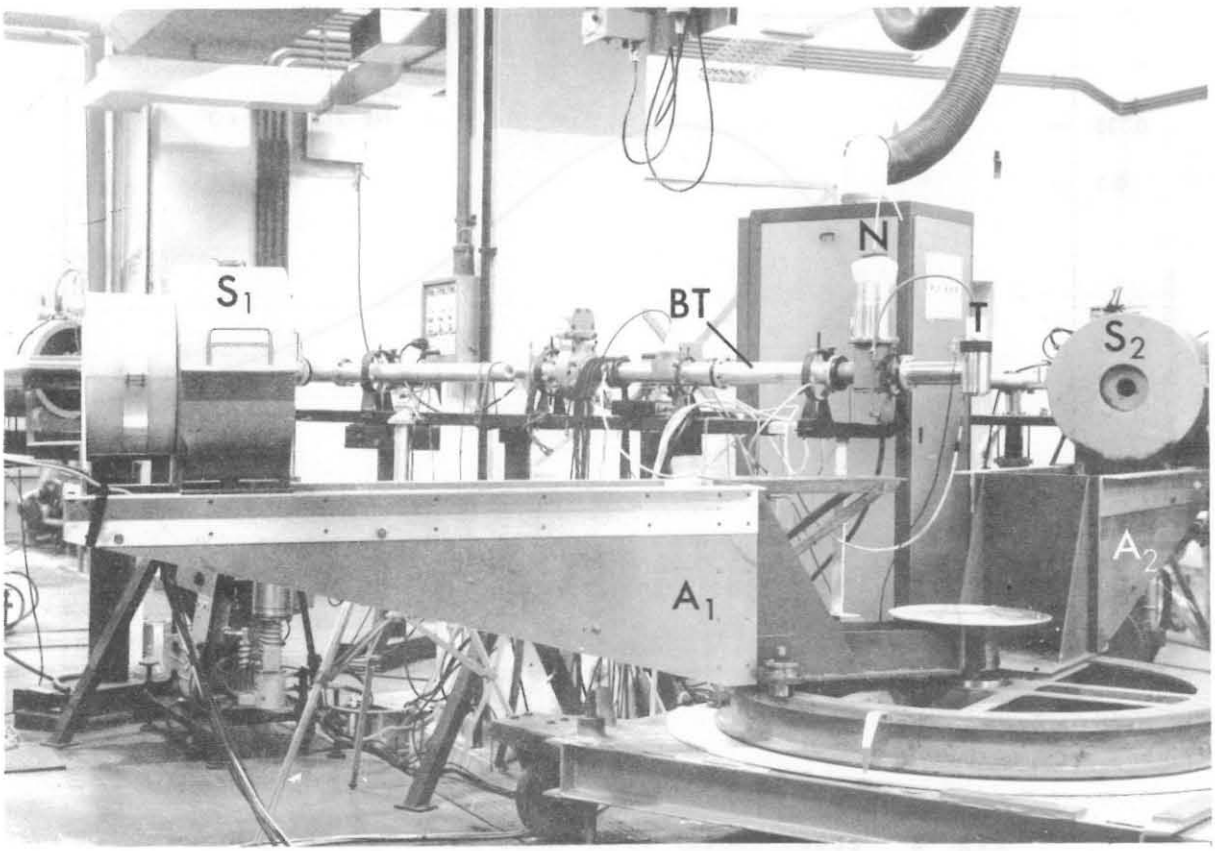

Fig. 1 - The target-detectors assembly used during the measurements on the $^{10}B(^{3}He;n)^{12}N$ reaction.
S_1 and S_2: neutron spectrometers.
T: ^{10}B target.
N: liquid nitrogen trap.
A_1 and A_2: rotating arms.
BT: accelerator beam tube.

(in Fig. 2 the efficiency curve for this spectrometer is reported) while the second spectrometer was placed at a fixed angle and used as a monitoring system to control the life of the target and the eventual deposits on it.

The ^{10}B target, prepared at the isotopic separator of Harwell with a thickness of 100 $\mu gr/cm^2$, was cooled by a stream of compressed air. This target, provided with an electric barrier, was connected to a current integrator. A cooling system around the beam, close to the target, was use to prevent carbon contaminations. The electronic circuits coupled to the detectors for the time-of-flight spectrometry, were conventional ORTEC instrumentation: the block diagram is shown in Fig. 3. In both the time-of-flight channels, the spectrometers gave the fast start signals and a

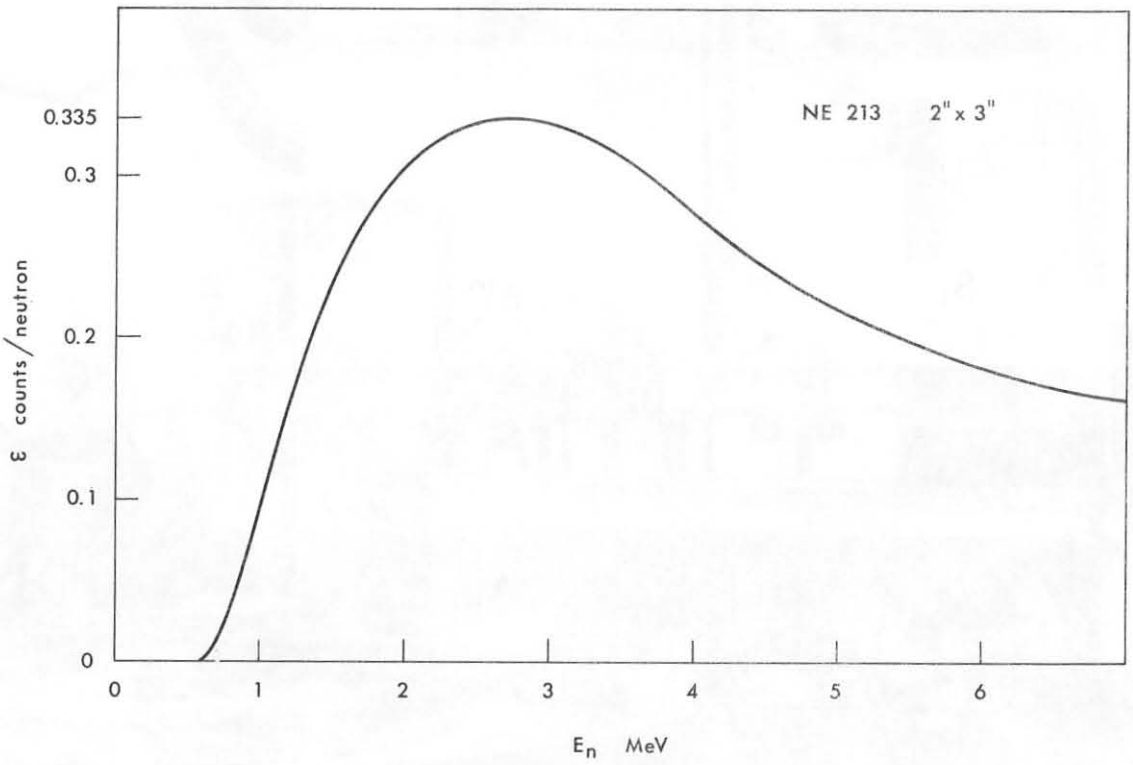

Fig. 2 - Spectrometer efficiency ε in the neutron energy range of the present measurements.

cilindrical pick-up surrounding the accelerator beam, gave the signal that, conveniently delayed, supplied the stop for the time analysis. In both the channels a pulse shape discrimination system was used in order to record only the events corresponding to the neutron detection. The time spectra obtained were calibrated observing the neutron groups from the ground states in the reactions $^{12}C(^{3}He;n)^{14}O$ (Q = - 1.148 MeV) and $^{16}O(^{3}He;n)^{18}Ne$ (Q = -2.980 MeV). The neutron spectra were measured at the energies of ^{3}He of 4.7 MeV and 5.5 MeV, for 14 and respectively 17 points in the angular range between 0° and 160°.

3. - DATA ANALYSIS

The Fig. 4 shows the $^{10}B(^{3}He;n)^{12}N$ time-of-flight spectrum at an energy of ^{3}He of 5.5 MeV and at an angle of 48.11° in the laboratory system. We can clarly observe several neutron groups, even not completely resolved, superimposed to a background arising from two contributions. The first contribution, continuous and constant is not directly caused

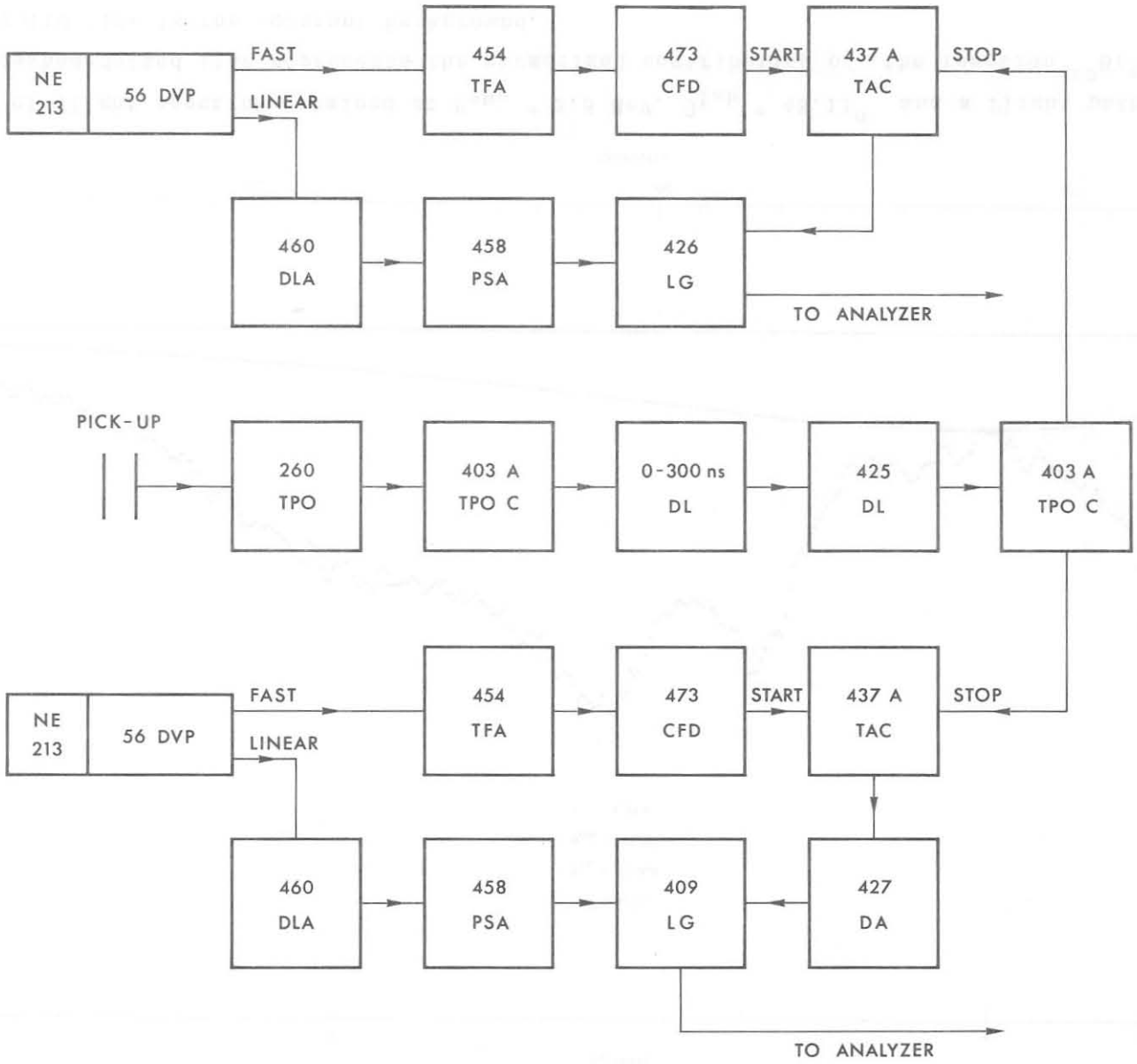

Fig. 3 - Block diagram of the spectrometers with the associated electronics.

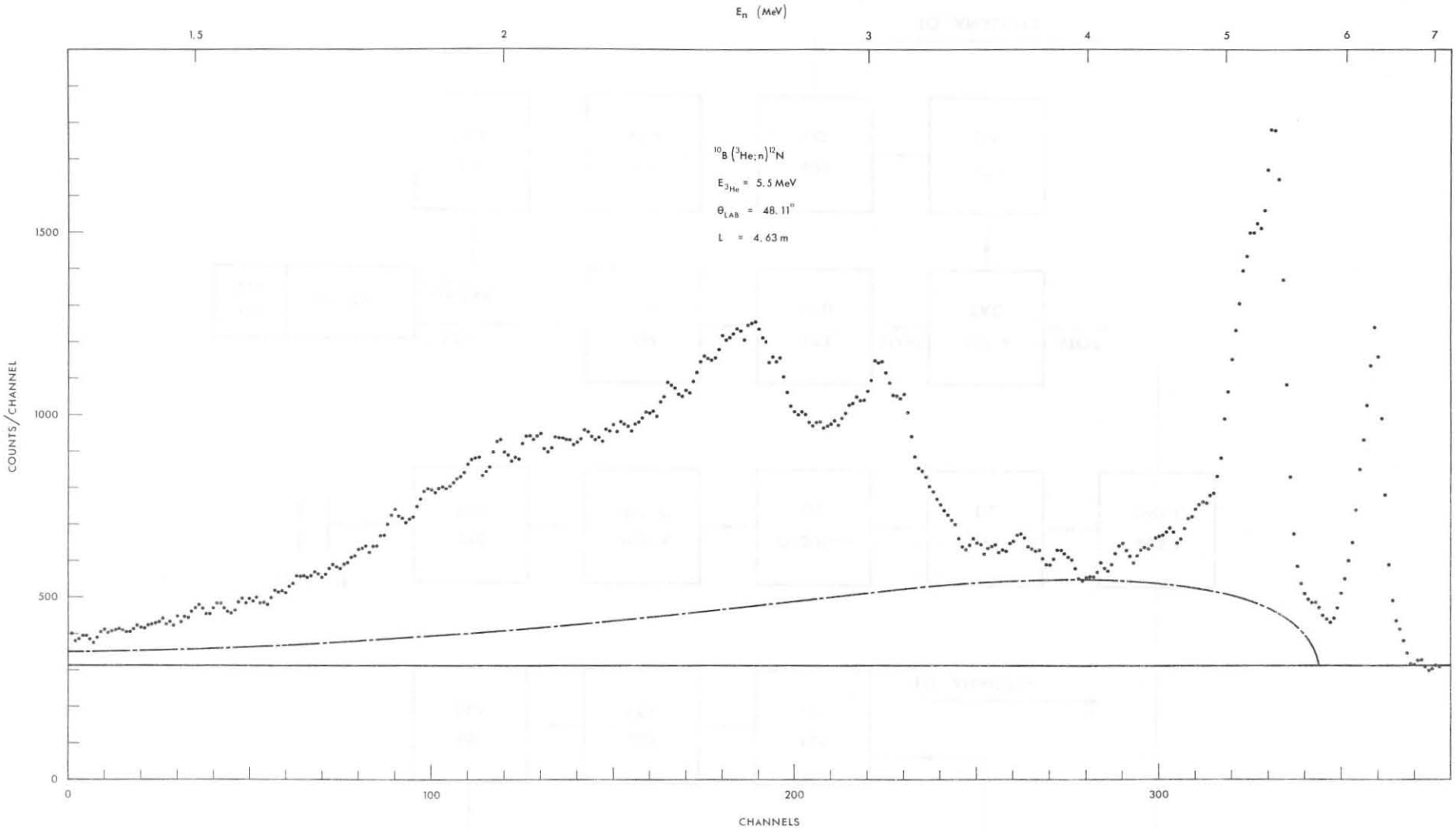

Fig. 4 - Time of flight spectrum obtained at $E_{^{3}He}$ = 5,5 MeV, θ_{lab} = 48,11° and a flight path L = 4,6 meters. The dashed-dotted line represents the normalized contribution of the reaction $^{10}B(^{3}He;np)^{11}C$. The solid line is the constant background.

by the target: it is due to the laboratory background and to the limits of the gamma-neutron discrimination. The second contribution arises from the reaction $^{10}B(^{3}He;n-p)^{11}C$, which originates neutrons with a maximum energy (11)

$$E_{max} = \left[a \cos\theta + (E_c - a^2 \sin^2\theta)^{\frac{1}{2}} \right]^2$$

with

$$a = \frac{(m_n \, m_{^3He} \, E_{^3He})^{\frac{1}{2}}}{m_{^3He} + m_{^{10}B}}$$

$$E_c = \frac{m_p + m_{^{11}C}}{m_n + m_p + m_{^{11}C}} \bar{E}_c$$

$$\bar{E}_c = Q + \frac{m_{^{10}B} \, E_{^3He}}{m_{^3He} + m_{^{10}B}}$$

In this particular case, it is $E_{max} = 5.699$ MeV. The recorded spectrum of the neutrons produced in the three body reaction is given by

$$F(\Omega_{np^{11}C} \, E_{np^{11}C}) = \frac{d^2\sigma}{d\Omega dE} \varepsilon \Delta E = \frac{8\pi^2}{\hbar^2} \frac{\mu}{K} \langle |M| \rangle^2 \rho(E) \, \varepsilon \Delta E$$

where

μ is the reduced mass of the system ^{3}He-^{10}B

$\hbar K$ is the relative momentum of ^{3}He and ^{10}B

$\langle |M| \rangle$ is the matrix element of the energy distribution averaged in the solid angle $\Omega_{p-^{11}C}$

$$\rho(E) = \frac{2(m_n + m_p + m_{^{11}C})^{\frac{1}{2}} (m_n m_p m_{^{11}C})^{\frac{3}{2}}}{(m_p + m_{^{11}C})} \left\{ E \left[\left(\frac{m_n}{m_p + m_{^{11}C}} + 1 \right)^{-1} \bar{E}_c - E + 2aE^{\frac{1}{2}} \cos\theta - a^2 \right] \right\}^{\frac{1}{2}}$$

ε is the detector efficiency

ΔE is the energy range corresponding to the width of a recording channel

Assuming the energy distribution of the neutrons as purely statistical the matrix element $\langle |M| \rangle$ is constant. The shape of the three body contribution calculated in this way is represented by the dashed-dotted line

in Fig. 4. For all the spectra, the constant background was assumed to be the incoherent contributions in the energy region where groups of neutrons do not appear. The total background is obtained by summing to this constant contribution the three body distribution normalized to the experimental data in the region of the spectrum where other decay channels are not present or contribute with a negligible intensity. The spectrum of the observed neutron rows is determined subtracting the total background from the experimental data. In order to obtain information on the energy of the maxima of the rows and on their widths and intensities from the analysis of this spectrum, the knowledge of the characteristic shape of the spectrometer response is required.

4. - STANDARD SHAPE OF THE SPECTROMETER RESPONSE

The analysis has started from those experimental rows related to the resolved neutron groups at various angles and energies. Converting the shape of the rows from the time of fligth scale (as stored in the channel analyzer at the exit of the time-to-amplitude converter) to the energy scale and correcting the experimental data for the efficiency ε and the energy range ΔE above defined, the shape reported in Fig. 5 has been obtained as standard response.

In this figure it is shown a row with a experimental width at half amplitude of $\Gamma_{exp} = 0.495$ MeV. It can be noticed that, fortunately, the spectrometers response in the energy scale is very simple: there are two linear shapes both for the rise and for the decay of the row. With reference to the parameters reported in Fig. 5, from our experimental data it has been obtained

$$\Gamma^{(1)} = 0.6061\ \Gamma_{tot}$$

$$\Gamma^{(2)} = 0.3939\ \Gamma_{tot}$$

$$\Gamma^{(1)} + \Gamma^{(2)} = \Gamma_{tot}$$

The row is described by two functions G(E) and F(E) where the demain

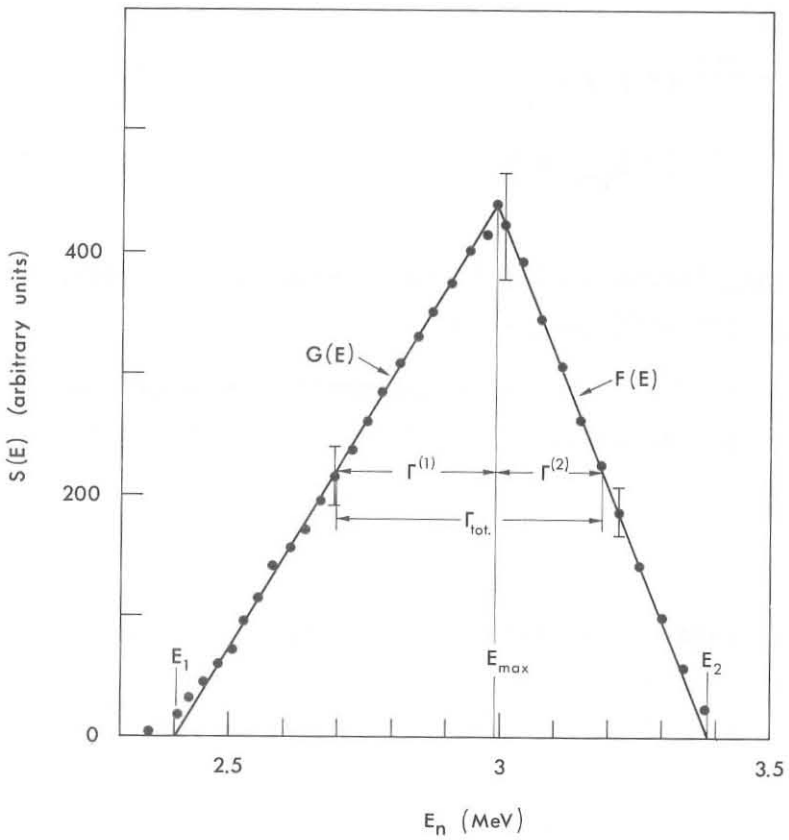

Fig. 5 - Spectrometer response shape derived from the experimental data and referred to the energy scale. The quantities reported in the figure are defined in the text.

of the former is the energy range E_1-E_{max} (where $E_1 = E_{max} - 2\,\Gamma^{(1)}$) while the demain of the latter is E_{max}-E_2 (where $E_2 = E_{max} + 2\Gamma^{(2)}$).

The above-mentioned functions are:

$$F(E) = \frac{H}{2\,\Gamma^{(2)}} \quad (E_{max}+2\Gamma^{(2)}-E)$$

$$G(E) = \frac{H}{2\,\Gamma^{(1)}} \quad (E - E_{max}+2\Gamma^{(1)})$$

that can be unified in a single analitical expression:

$$S(E) = 1 - \frac{(E_{max}-E)^2}{2\Gamma^{(i)}|E-E_{max}|}$$

with $S(E) \geq 0$

$$\Gamma^{(i)} = \Gamma^{(1)} \quad \text{if } E \leq E_{max}$$

$$\Gamma^{(i)} = \Gamma^{(2)} \quad \text{if } E_{max} \leq E$$

The above defined function $S(E)$ is calculated in the energy scale and for a detector with efficiency $\varepsilon = 1$.

To transform $S(E)$ into the experimental shape of the row $S_{exp}(E)$ measured with the time of flight analysis, we have to write

$$S_{exp}(E) = S(E) \cdot \varepsilon \cdot \Delta E$$

The energy range ΔE, expressed in MeV, corresponding to a channel of the recording system, can be related to the temporal lenght in nsecs, Δt of the same channel by the function

$$\Delta E = - \frac{2}{KL} E^{3/2} \Delta t$$

where $K = 72.3 \frac{ns\ (MeV)^{\frac{1}{2}}}{m}$

and L is the flight path in meters.

Therefore, the following explicit expression for the experimental shape of the row is obtained

$$S_{exp}(E) = \left[1 - \frac{(E_{max}-E)^2}{2\Gamma^{(i)}|E-E_{max}|} \right] \frac{2\,\Delta t}{KL} E^{3/2} \varepsilon(E)$$

with

$$S_{exp}(E) \geq 0$$

$$\Gamma^{(i)} = 0.6061\ \Gamma_{tot} \quad \text{if } E \leq E_{max}$$

$$\Gamma^{(i)} = 0.3939\ \Gamma_{tot} \quad \text{if } E \geq E_{max}$$

In Fig. 6 the function $S_{exp}(E)$ is reported with the experimental points of the row.

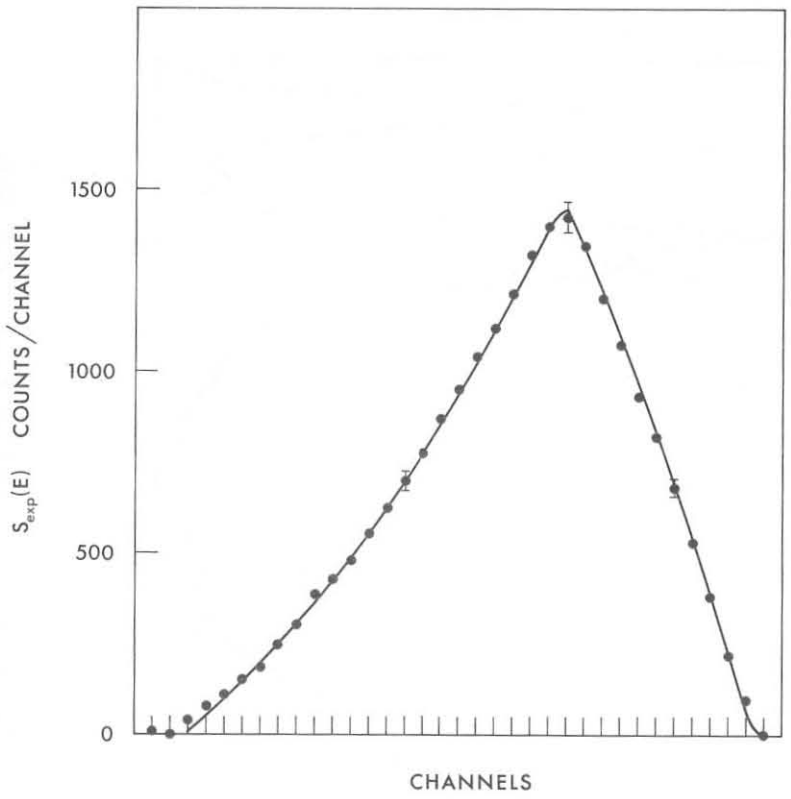

Fig. 6 - Calculated shape for the time of flight spectrometer response compared with the experimental points.

5. - FIT OF THE CALCULATED SPECTROMETER RESPONSES TO THE EXPERIMENTAL SPECTRA

The position in the time-of-flight spectrum of a neutron row depends on the source reaction and its Q-value or, in other words on the excitation energy of the residual nucleus relative level and incident particle energy.

The row shape, if the spectrometer response $S_{exp}(E)$ is known, depends on the experimental total width Γ_{tot},

$$\Gamma_{tot} = (\Gamma_{group}^{2} + \Gamma_{burst}^{2})^{\frac{1}{2}}$$

where Γ_{group} corresponds, in the laboratory reference system (L.S.), to Γ_{CM}, which is the width in the center of mass system (CMS) of the residuam nucleus level corresponding to the observed neutron group. Γ_{burst} is the width of the spectrometer response for a neutron row corresponding to a

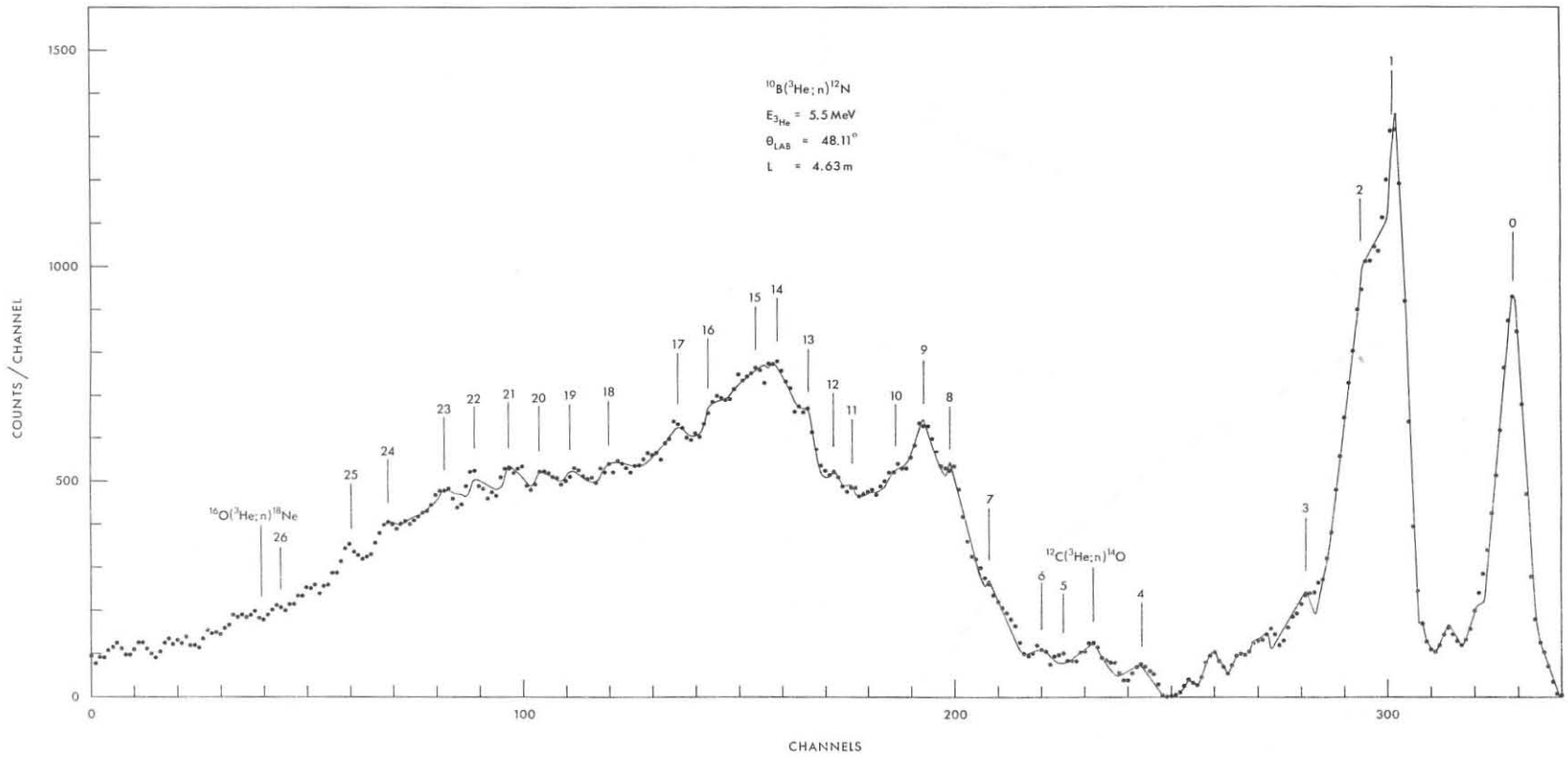

Fig. 7 - Time of flight spectrum for the reaction $^{10}B(^{3}He;n)^{12}N$ obtained at $E_{^{3}He}$ = 5,5 MeV, θ_{lab} = 48,11° and L = 4,6 meters after the background subtraction. The solid line is the best fit to the experimental data with 30 row shapes. The neutron rows are enumerated in the order of the increasing excitation energies.

nuclear level with $\Gamma_{CM} = 0$. Γ_{burst} practically depends on the accelerator burst duration, therefore it is a constant for all the time of flight spectrum. Γ_{tot} is defined in the L.S., then it depends on the incident ^3He energy and on the observation angle, besides on the above considered reaction parameters. Thus, when the positions of the rows in the spectrum at a certain energy and angle are determined, by changing one ore both of these parameters, Γ_{tot} will change. Our analysis of the experimental data has started from the neutron time-of-flight spectrum of Fig. 7. Here some neutron groups can be seen. After the identification of the rows arising from the target contaminations of carbon and oxigen, we have subtracted the background structures arising from the laboratory contributions that have been determined with a tantalum target with the same charge collection as used in the study of the $^{10}B(^3He,n)^{12}N$ reaction. The remaning rows have been attributed to the $^{10}B(^3He,n_i)^{12}N$ reaction. This assignment has been considered as definitive only for those rows which obey, for position and width in the spectra, the kinematical relations in the other 34 spectra obtained at various angles between 0 and 160 degrees at the ^3He energies of 4.7 MeV and 5.5 MeV. Then a procedure of experimental data reproduction has started for the spectra obtained at different energies and angles, by imposing the row shapes $S_{exp}(E)$ calculated in the previous section, in a best fit with 30 rows. This calculation has been performed at the HP2100S computer of the Istituto di Fisica dell'Università di Trieste. The experimental widths Γ_{tot} have been determined by an iterative method assuming the variance as a parameter for the goodnes of the computation. This procedure has been followed even for the spectrum intervals with not completely resolved rows. During this elaboration we have imposed the obvious condition that Γ_{CM} remains constant for each neutron row. The relation between Γ_{CM} and the experimental Γ_{group} is

$$\Gamma_{CM} = M_1 \Gamma_{group} - \frac{1}{2}\left[M_1 E_{max} - M_2 E_{^3He} - Q\right]\left[\left(1+\frac{a\,\Gamma_{group}}{2\,E_{max}}\right)^{\frac{1}{2}} - \left(1-\frac{b\,\Gamma_{group}}{2\,E_{max}}\right)^{\frac{1}{2}}\right] \quad (1)$$

where

$$M_1 = 1+\frac{m_n}{m_{^{12}N}} \qquad M_2 = 1-\frac{m_{^3He}}{m_{^{12}N}}$$

$$a = 0.3939 \qquad b = 0.6061 \qquad a + b = 1$$

6. - RESULTS

The energies of the row maxima have been obtained from the experimental spectra analysis with the method described in the previous sections, at different emission angles and ^3He energies. The Q-values and the level excitation energies E_x have been deduced from these data. The differential cross sections in the C.M.S. have been obtained from the analysis of the row intensities. These data are collected in the tables from 1 to 6 together with the ^3He energies $E_{^3He}$ and the observation angles θ_{lab} in the L.S. and θ_{CM} in the C.M.S. The errors reported in these tables are comprehensive of those due to the spectrometer efficiency determination, to the monitoring system, to the incoherent background contribution, to the $^{10}B(^3He;np)^{11}C$ reaction contribution and to the superposition of different rows. The level widths T_{CM} obtained in this work are reported in Tab. 7: as they have been deduced from the best fit of the row shapes to the experimental data. In this table our results are compared with the level parameters of ^{12}B and ^{12}C, that are the other members of the A = 12 isobaric triad.

In Fig. 7 a comparison is made between the experimental spectrum (obtained at $E_{^3He}$ = 5,5 MeV, θ_{lab} = 48, 11° and L = 4.6 meters, and already submitted to the backgrounds subtraction) and the spectrum calculated with the parameters of Tab. 7. The numbers on the rows correspond to the increasing excitation energies.

The differential cross section for the $^{10}B(^3He;np)^{11}C$ reaction in the neutron energy range from 0,7 MeV to the maximum possible energy for different θ_{lab} at $E_{^3He}$ = 5.5 MeV is shown in Tab. 8 and in Fig. 15. All the experimental differential cross sections obtained in this work and presented in the tables from Tab. 1 to Tab. 6 are displayed in the figures from Fig. 8 to Fig. 14.

The experimental angular distributions, obtained at $E_{^3He}$ = 4,7 MeV and $E_{^3He}$ = 5,5 MeV, for the neutrons from the ground, the first (E_x = 977±14 keV) and the second (E_x = 1215±23 keV) excited state of ^{12}N have been compared with those calculated assuming that both direct reaction and compound nucleus reaction are present in the $^{10}B(^3He;n)^{12}N$ reaction. The direct interaction has been interpreted

TABLE 1 - DIFFERENTIAL CROSS SECTIONS FOR THE $^{10}B(^{3}He,n)^{12}N$ REACTION (μb/sr)

	$E_{^3He}$ = 4.7 MeV							
θ°_{LAB}	E_x = 0 (g.s.)		E_x = 0.977 MeV		E_x = 1.215 MeV		E_x = 1.565 MeV	
	θ°_{CM}	$\frac{d\sigma}{d\Omega}$	θ°_{CM}	$\frac{d\sigma}{d\Omega}$	θ°_{CM}	$\frac{d\sigma}{d\Omega}$	θ°_{CM}	$\frac{d\sigma}{d\Omega}$
0	0	479±31	0	544±37	0	107±12	0	42±8
15	16.99	456±63	17.20	493±75	17.25	299±52	17.3	46±22
30	33.85	420±60	34.25	537±82	34.35	425±68	34.44	50±23
45	50.44	423±65	51.02	590±85	51.16	269±47	45.71	77±24
60	66.67	386±58	67.38	625±85	67.55	52±21	67.71	91±24
75	82.45	347±55	83.24	518±75	83.42	0	83.61	99±25
90	97.71	281±47	98.53	386±57	98.72	50±18	98.91	52±18
110	117.24	320±51	118.01	423±62	118.19	313±49	118.37	37±18
120	126.67	329±52	127.38	491±67	127.55	172±35	127.71	53±21
130	135.90	307±49	136.52	490±70	136.67	264±45	136.82	37±19
145	149.41	274±45	149.88	436±66	149.99	255±44	150.10	72±23
150	153.85	252±42	154.25	384±59	154.35	245±43	154.44	53±21
160	162.63	209±36	162.91	309±50	162.97	284±47	163.04	49±21

TABLE 2 - DIFFERENTIAL CROSS SECTIONS FOR THE $^{10}B(^{3}He,n)^{12}N$ REACTION (μb/sr)

	$E_{^3He}$ = 5.5 MeV							
θ°_{LAB}	E_x = 0 (g.s.)		E_x = 0.977 MeV		E_x = 1.215 MeV		E_x = 1.565 MeV	
	θ°_{CM}	$\frac{d\sigma}{d\Omega}$	θ°_{CM}	$\frac{d\sigma}{d\Omega}$	θ°_{CM}	$\frac{d\sigma}{d\Omega}$	θ°_{CM}	$\frac{d\sigma}{d\Omega}$
0	0	891±91	0	418±43	0	476±53	0	74±16
10	11.33	793±81	11.48	528±53	11.51	440±63	11.6	66±22
20	22.63	700±71	22.91	448±46	22.97	618±65	23.16	82±36
40	44.95	607±62	45.47	592±60	45.59	447±60	45.95	55±12
60	66.67	430±44	67.38	459±47	67.55	307±57	68.03	45±9
80	87.59	387±40	88.40	460±48	88.59	152±20	89.14	22±10
100	107.59	420±43	108.40	535±54	108.59	264±29	109.14	17±13
120	126.67	390±40	127.38	566±58	127.55	236±27	128.03	25±8
140	144.95	274±29	145.47	474±49	145.59	191±23	145.95	19±8
160	162.63	194±20	162.91	340±36	162.97	354±41	163.13	1±1
0	0	813±132	0	534±111	0	420±94		
15	17	760±125	17.2	541±109	17.3	885±156		
30	33.9	603±100	34.3	530±104	34.4	812±142		
45	50.5	566±92	51.1	442±86	51.2	649±113		
60	66.8	445±72	67.4	346±69	67.6	453±81		
75	82.5	356±56	83.3	379±63	83.5	379±61		
90	97.8	360±54	98.6	527±77	98.8	227±43		
105	112.5	440±59	113.3	586±78	113.5	386±58		
120	126.8	381±48	127.4	626±75	127.6	455±58		
135	140.5	313±40	141.1	684±78	141.2	408±53		
140	145.0	289±39	145.5	610±73	145.6	403±54		

TABLE 2 - The data of neutron differential cross sections here reported derive from two different measurements.

TABLE 3 - DIFFERENTIAL CROSS SECTIONS FOR THE $^{10}B(^{3}He,n)^{12}N$ REACTIONS (μb/sr)

θ°_{LAB}	$E_{^3He}$ = 5.5 MeV									
	E_x = 2.410 MeV		E_x = 2.723 MeV		E_x = 2.801 MeV		E_x = 2.983 MeV		E_x = 3.108 MeV		E_x = 3.188 MeV	
	θ°_{CM}	$\frac{d\sigma}{d\Omega}$	θ°_{CM}	$\frac{d\sigma}{d\Omega}$	θ°_{CM}	$\frac{d\sigma}{d\Omega}$	θ°_{CM}	$\frac{d\sigma}{d\Omega}$	θ°_{CM}	$\frac{d\sigma}{d\Omega}$	θ°_{CM}	$\frac{d\sigma}{d\Omega}$
0			0	15±8			0	47±9	0	184±21	0	191±28
10	11.78	19±7	11.86	46±9			11.94	67±10	11.99	121±15	12.01	197±22
20	23.51	10±7					23.82	49±8	23.92	108±13	23.97	165±19
40							47.20	51±9	47.39	128±15	47.48	83±11
60	68.91	14±6			69.46	17±6	69.72	93±12	69.97	121±15	70.10	70±10
80			90.62	16±7	90.77	12±6	91.07	70±11	91.36	142±17	91.50	69±10
100			110.62	29±8	110.77	21±7	111.07	119±12	111.36	153±18	111.50	135±17
120			129.32	60±11	129.46	19±8	129.72	114±16	129.97	208±24	130.10	100±14
140	146.60	36±9	146.91	43±11	147.01	34±9	147.20	148±19	147.39	193±24	147.48	48±14
160	163.51	8±8	163.67	30±10	163.72	44±11	163.82	131±19	163.91	161±22	163.97	97±16

TABLE 4 - DIFFERENTIAL CROSS SECTIONS FOR THE $^{10}B(^{3}He,n)^{12}N$ REACTIONS (μb/sr)

θ°_{LAB}	$E_{^3He}$ = 5.5 MeV									
	E_x = 3.277 MeV		E_x = 3.395 MeV		E_x = 3.3442 MeV		E_x = 3.507 MeV		E_x = 3.588 MeV		E_x = 3.633 MeV	
	θ°_{CM}	$\frac{d\sigma}{d\Omega}$	θ°_{CM}	$\frac{d\sigma}{d\Omega}$	θ°_{CM}	$\frac{d\sigma}{d\Omega}$	θ°_{CM}	$\frac{d\sigma}{d\Omega}$	θ°_{CM}	$\frac{d\sigma}{d\Omega}$	θ°_{CM}	$\frac{d\sigma}{d\Omega}$
0	0	125±14	0	106±13	0	44±5	0	149±20	0	316±33	0	168±19
10	12.04	94±12	12.09	248±27			12.16	282±30	12.18	93±12	12.20	243±26
20	24.02	97±12	24.11	203±22			24.25	175±19	24.30	210±23	24.34	118±14
40	47.57	111±14	47.75	54±9	47.84	106±13	48.01	31±6	48.10	238±25	48.18	36±7
60	70.22	54±8	70.47	102±13	70.59	82±11	70.82	46±8	70.94	154±18	71.05	63±9
80	91.64	95±13	91.92	144±18	92.06	42±8	92.33	66±10	92.46	192±22	92.59	7±6
100	111.64	63±11	111.92	213±25	112.06	52±10	112.33	60±10	112.46	241±27	112.59	33±8
120	130.22	90±14	130.47	282±32	130.59	71±18	130.82	80±13	130.94	307±35	131.05	50±11
140	147.57	121±17	147.75	291±35	147.84	52±12	148.01	99±16	148.10	299±36	148.18	32±12
160	164.02	86±16	164.11	244±32	164.16	75±15	164.25	117±19	164.30	363±44	164.34	90±19

TABLE 5 - DIFFERENTIAL CROSS SECTIONS FOR THE $^{10}B(^{3}He,n)^{12}N$ REACTIONS (μb/sr)

θ°_{LAB}	$E_{^3He}$ = 5.5 MeV									
	E_x = 3.739 MeV		E_x = 3.803 MeV		E_x = 3.938 MeV		E_x = 4.006 MeV		E_x = 4.061 MeV		E_x = 4.111 MeV	
	θ°_{CM}	$\frac{d\sigma}{d\Omega}$	θ°_{CM}	$\frac{d\sigma}{d\Omega}$	θ°_{CM}	$\frac{d\sigma}{d\Omega}$	θ°_{CM}	$\frac{d\sigma}{d\Omega}$	θ°_{CM}	$\frac{d\sigma}{d\Omega}$	θ°_{CM}	$\frac{d\sigma}{d\Omega}$
0	0	316±33	0	63±9	0	290±31	0	19±5	0	114±13	0	13±5
10	12.27	309±32	12.31	93±11	12.38	249±27	12.44	102±12			12.50	152±17
20	24.47	301±32	24.56	62±9	24.68	239±26	24.81	37±6	24.89	107±13	24.92	15±5
40	48.43	280±30	48.59	40±7	48.83	245±26	49.06	64±9	49.21	63±9	49.28	39±7
60	71 39	236±26	71.61	54±8	71.93	259±28	72.25	83±11	72.45	31±6	72.55	103±13
80	92.98	341±37	93.23	31±7	93.60	360±39	93.96	89±12	94.19	50±9	94.31	103±14
100	112.98	455±49	113.23	43±9	113.60	469±51	113.96	66±12	114.19	71±13	114.31	111±16
120	131.39	576±62	131.61	33±11	131.93	523±59	132.25	105±18	132.45	117±20	132.55	162±25
140	148.43	587±66	148.59	24±14	148.83	596±71	149.06	72±23	149.21	81±25		
160	164.47	1311±139	164.56	53±20	164.68	579±77	164.81	104±33	164.89	146±39	164.92	196±49

TABLE 6 - DIFFERENTIAL CROSS SECTIONS FOR THE $^{10}B(^{3}He,n)^{12}N$ REACTIONS (μb/sr)

θ°_{LAB}	$E_{^3He}$ = 5.5 MeV									
	E_x = 4.164 MeV		E_x = 4.212 MeV		E_x = 4.293 MeV		E_x = 4.344 MeV		E_x = 4.431 MeV	
	θ°_{CM}	$\frac{d\sigma}{d\Omega}$	θ°_{CM}	$\frac{d\sigma}{d\Omega}$	θ°_{CM}	$\frac{d\sigma}{d\Omega}$	θ°_{CM}	$\frac{d\sigma}{d\Omega}$	θ°_{CM}	$\frac{d\sigma}{d\Omega}$
0	0	87±11	0	128±14	0	112±13	0	113±13	0	156±17
10			12.46	166±18	12.65	131±15	12.71	85±10	12.78	182±20
20	25.04	55±8	24.85	118±14	25.23	96±11	25.34	88±11	25.48	100±12
40	49.51	76±10	49.13	133±15	49.86	111±13	50.07	73±9	50.34	111±13
60	72.86	74±10	72.35	118±14	73.34	99±12	73.63	45±8	74.00	56±8
80	94.66	81±12	94.08	135±17	95.21	136±17	95.54	90±13	95.96	300±30
100	114.66	125±18	114.08	47±12	115.21	147±21	115.54	118±20	115.96	178±29
120			132.35	252±35	133.34	224±37	133.63	209±38	134.00	334±68
140	149.51	192±39	149.13	149±40	149.86	163±55				
160	165.04	176±57	164.85	131±64						

TABLE 7 - ENERGY LEVELS OF A = 12 ISOBARIC TRIPLET

^{12}B			^{12}C			^{12}N (previous results)			^{12}N (present results)		
E_x (MeV±KeV)	J^π	Γc.m. (KeV)	E_x (MeV±KeV)	J^π	Γc.m. (KeV)	E_x (MeV±KeV)	J^π	Γc.m. (KeV)	E_x (MeV±KeV)	J^π	$\Gamma_{c.m.}$ (KeV)
g.s.	1^+	bound	15,110 ±3	1^+	42±7 eV	g.s.	1^+	bound	g.s.	1^+	bound
0,9531±0.60	2^+	bound	16,1067±0.5	2^+	6,5±0,6	0,964±8	2^+	<35 KeV	0,977±14	2^+	≤20
1,6736±0.60	2^-	bound	16,58	2^-	300	1,192±9	$(2)^-$	140±30	1,215±23	2^-	140±30
						(1,72±0.08)			1,565±80		≤40
2,6208±1.2	1^-	bound	17,23	1^-	1150	2,415±20		45±15	2,410±20		≤50
2,723 ±11	0^+	bound	17,76 ±20	0^+	80±20				2,723±14		120±20
									2,801±80		≤40
			18,13	(1^+)	600±100				2,983±80		100±60
						3.114±15	π = +	210±50	3,108±11		100±30
			(18,27±50)	(4^-)	257±40				3,188±11		≤40
			18,36±50	(3^-)	210±40				3,277±80		80±60
3,3884±1.4	3^-	3.1±0.6eV	18,40±60	0^-	43				3,395±13		180±30
									3,442±80		≤40
			(18,6±100)	(3^-)	300				3,507±12		≤40
			18,71	π = +	100				3,588±11		90±20
									3,633±80		≤40
3,759 ±6.	2^+	37±5	18,80±40	2^+	80±30	3.533±15	$(2)^+$	170±50	3,739±11		180±30
									3,803±11		≤40
									3,938±12		190±30
									4,006±12		≤40
									4,061±80		≤40
			19,25	(1^-)	1100				4,111±80		≤40
									4,164±11		≤40
						4,25 ±30		290±70	4,212±80		≤40
4,302 ±6	1^-	9±4	19±40	(2^+)	45				4,293±80		≤40
4,37	2^-	broad	19,57±40	(4^-)	400±60				4,344±10		≤40
			19,69		180						
4,521± 7	4^-	110±20	20,0	(2^+)	90				4.431±11		100±20
			20,24		170						
4,99 ±15	1^+	50±15	20,5	(3^+)	∿250	5,320±12		180±20	5.362±20		160±60
5,607± 7	3^+	110±20	20,6	(3^-)	200±40						
5,725± 7	3^-	60±15	20,98		270						

TABLE 7 - The data for the ^{12}B and the ^{12}C are derived from refs. (1)(2). The previous results from refs. (1)(2)(7)(8)(9)(10).

TABLE 8 - DIFFERENTIAL CROSS SECTIONS FOR THE $^{11}B(^{3}He,np)^{11}C$ REACTION (μb/sr).

$E_{^3He}$ = 5.5 MeV	
θ°_{LAB}	$\frac{d\sigma}{d\Omega}$ (μb/stern)
0	1493 ± 168
10	1603 ± 176
20	1505 ± 167
40	1309 ± 148
60	872 ± 110
80	918 ± 112
100	733 ± 98
120	641 ± 64
140	488 ± 78
160	458 ± 77

in terms of the distorted wave Born approximation (DWBA). For a target nucleus as the ^{10}B, with $J^{\pi} = 3^{+}$ thi approximation does not give the spin and parity of the residual nucleus levels. In fact, the shape of the calculated angular distributions for the two-proton transfer is depending, in the DWBA, on the value of the transferred total angular momentum; therefore the DWBAdoes not permit an unique spin determination for the levels of the residual nucleus if the target nucleus has spin different from zero. Further information are then required for the assignement. The comparison between the experimental and the calculated angular distributions has been performed by means of the relation

$$\frac{d\sigma}{d\Omega}_{exp} = C\, D^2\, \frac{2J_Y+1}{(2J_x+1)(2J_T+1)} \left[\frac{d\sigma}{d\Omega}_{DWBA} + F \frac{d\sigma}{d\Omega}_{CN} \right] \qquad (1)$$

The expression in the square braket gives the angular distribution for the double stripping process in DWBA, the term $\frac{d\sigma}{d\Omega}_{CN}$ represents the differential cross section calculated by means of the statistical

theory of compound nucleus. J_X, J_Y, J_T are the initial, final and transferred angular momentum respectively. The constants CD^2 and F are the parameters that best fit the calculated angular distributions to the experimental differential cross sections. For the determination of the double stripping angular distributions with the distorted waves we have used the zero range option of the DWBA computer programme DWUCK[12]. The compund nucleus differential cross sections have been

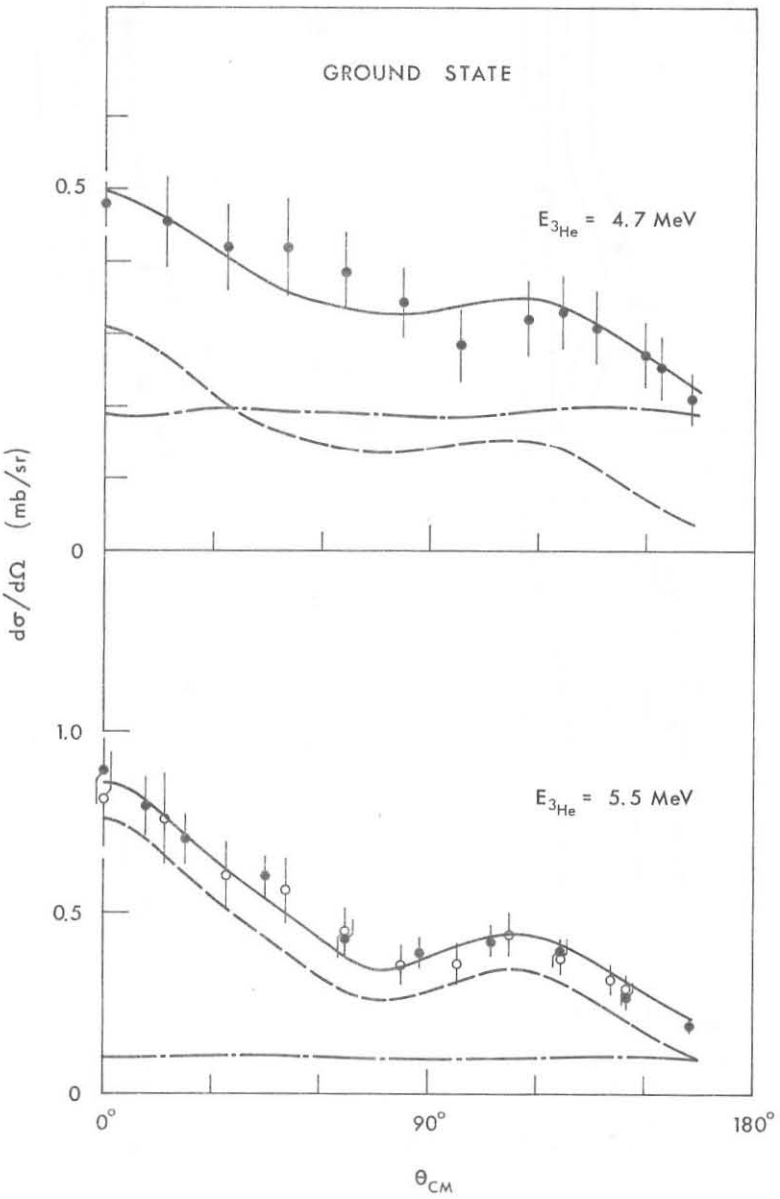

Fig. 8 - Experimental differential cross sections and calculated angular distributions for neutrons from the ground state of ^{12}N at $E_{^3He}$ = 4,7 MeV and $E_{^3He}$ = 5,5 MeV. The dashed line represents the DWBA contribution and the dashed-dotted line the CN contribution. The solid line is the sum of the two contributions.

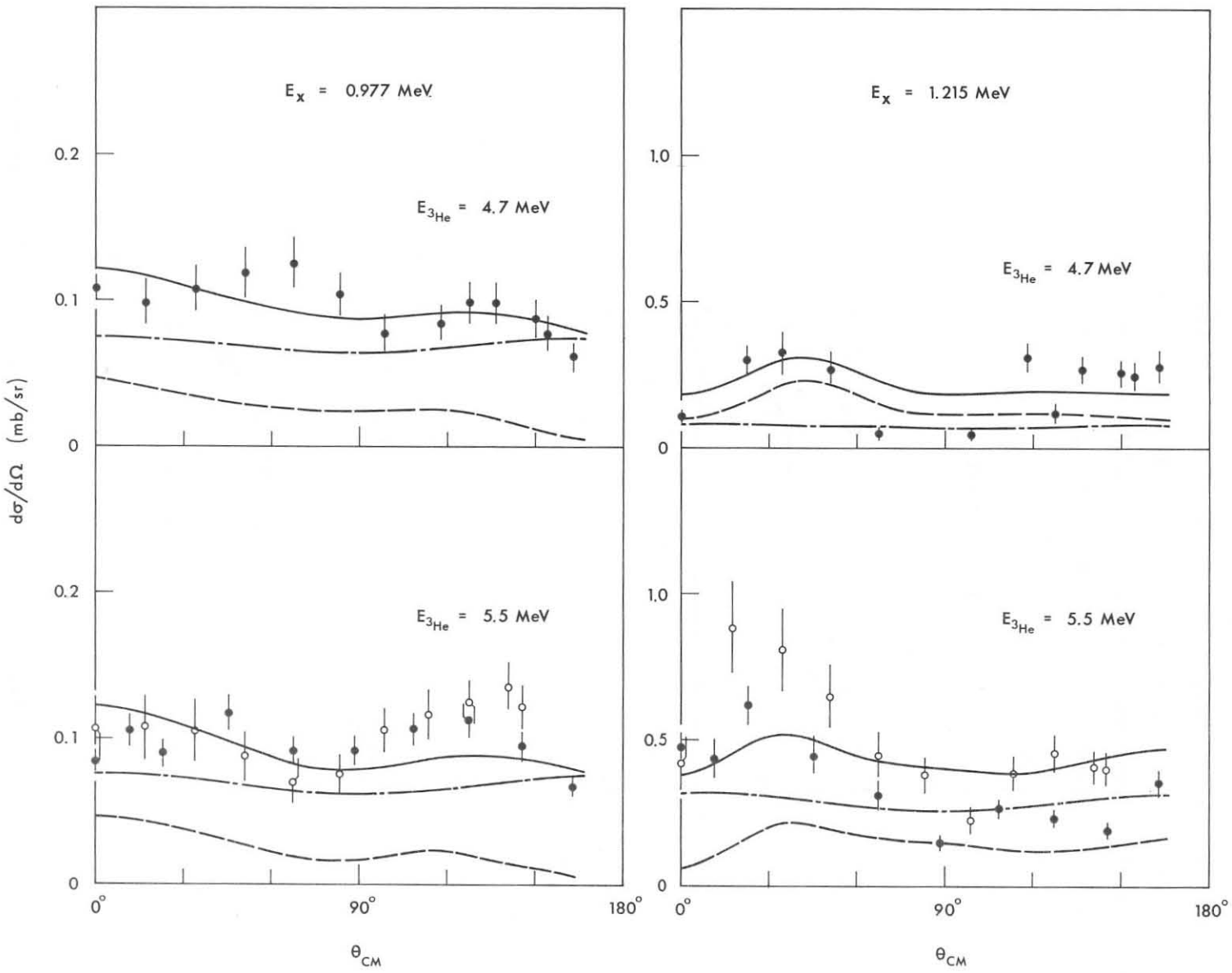

Fig. 9 - Experimental differential cross sections and calculated angular distributions for neutrons from the first E_x=0,977 MeV and the second E_x=1,125 MeV excited level of the ^{12}N at $E_{^3He}$=4,7 MeV and $E_{^3He}$=5,5 MeV. The dashed line represents the DWBA contribution and the dashed-dotted line the CN contribution. The solid line is the sum of the two contributions.

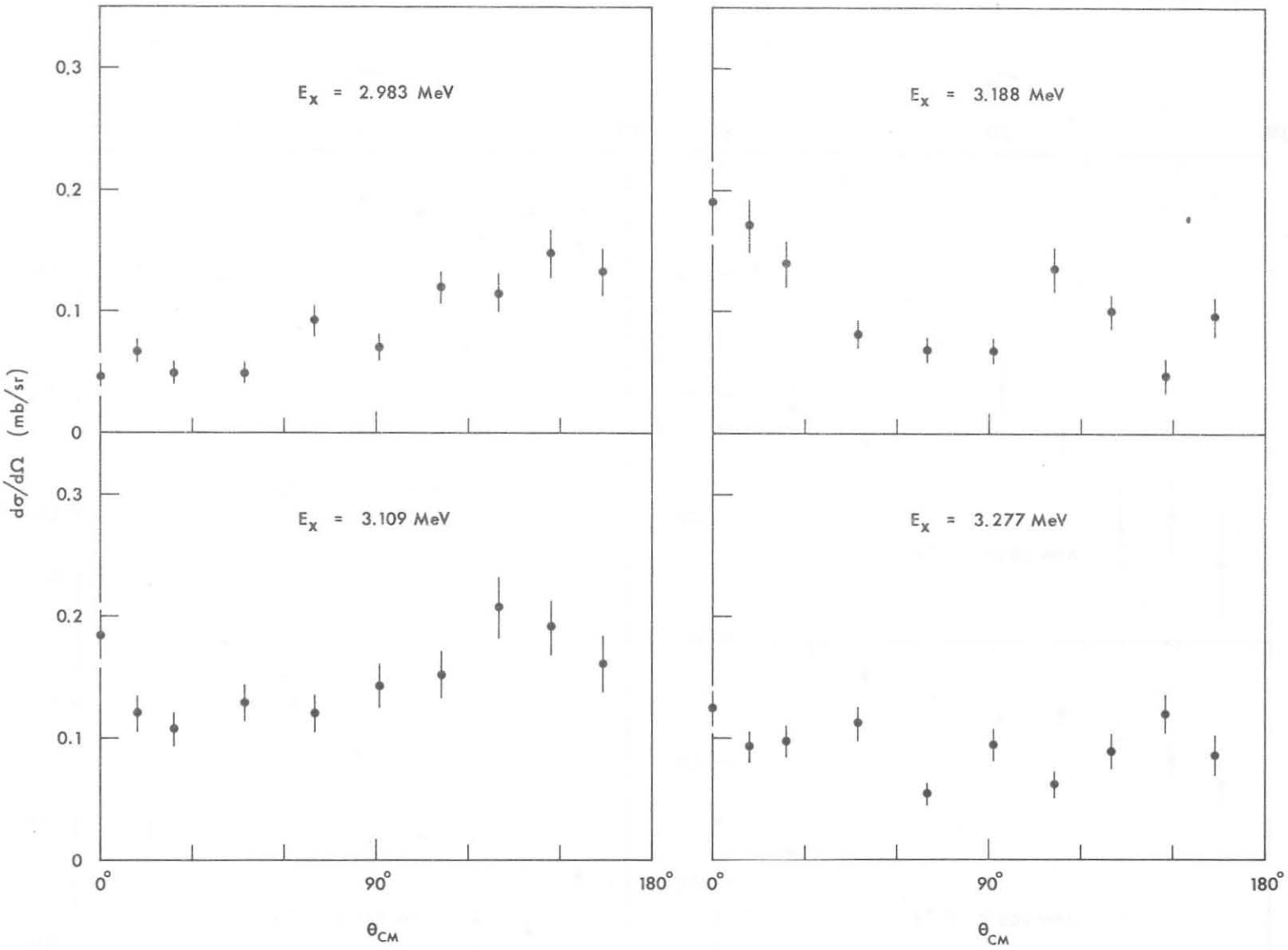

Fig. 10 - Neutron experimental differential cross sections obtained from the analysis with the row shapes for four ^{12}N levels at the excitation energies E_x reported in the figures.

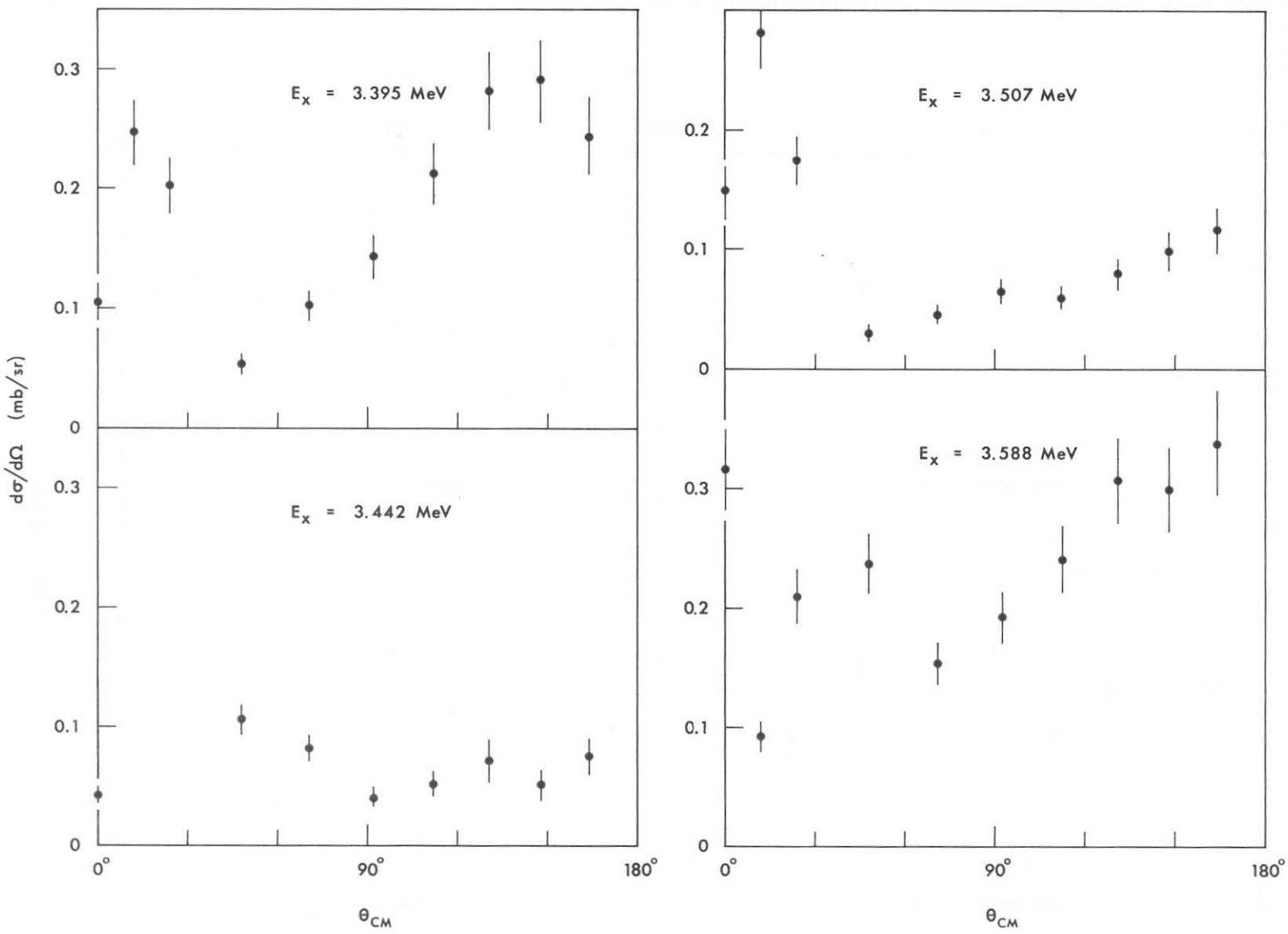

Fig. 11 - Neutron experimental differential cross sections obtained from the analysis with the row shapes for four ^{12}N levels at the excitation energies E_x reported in the figures.

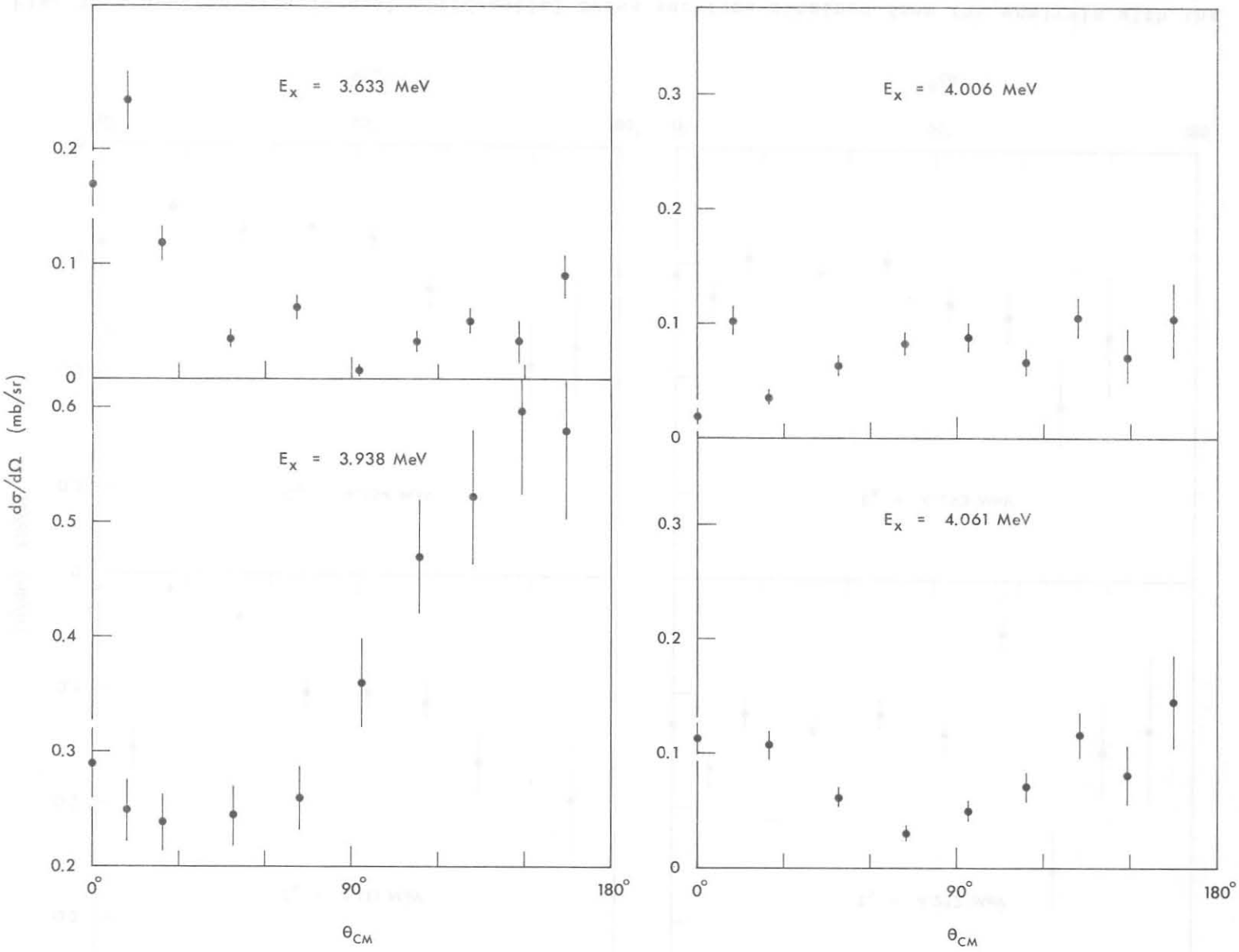

Fig. 12 - Neutron experimental differential cross sections obtained from the analysis with the row shapes for four ^{12}N levels at the excitation energies E_x reported in the figures.

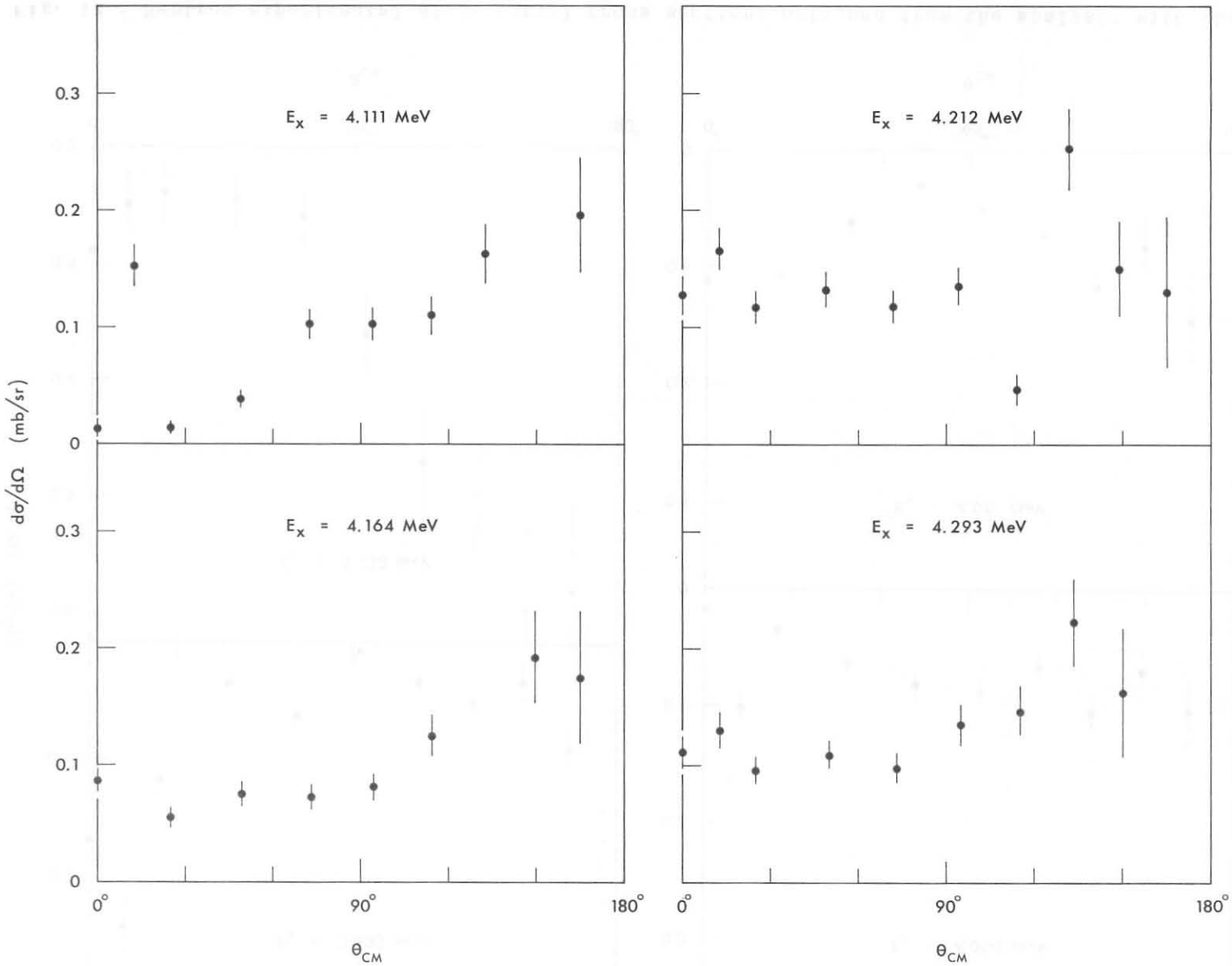

Fig. 13 - Neutron experimental differential cross sections obtained from the analysis with the row shapes for four ^{12}N levels at the excitation energies E_x reported in the figures.

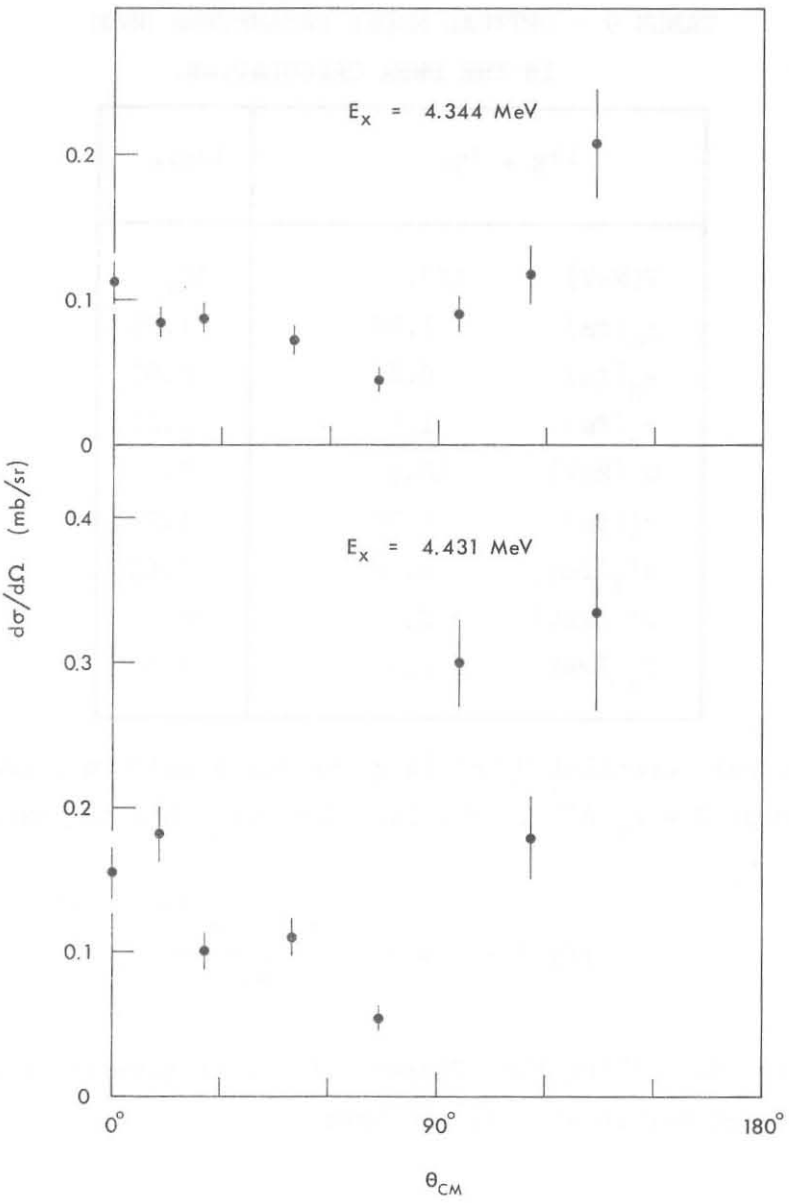

Fig. 14 - Neutron experimental differential cross sections obtained from the analysis with the row shapes for two ^{12}N levels at the excitation energies E_x reported in the figure.

calculated by means of the programme MANDY,[13] taking into account the contribution of 86 extra exit channels. The best agreement between the experimental and calculated data has been reached using the optical model parameters of Tab. 9. These values for the entry and exit channels have been used in the final calculations and are relative, for the DWBA, to the optical model potential

$$U(r) = U_c(r)+Vf(x_R)+iWf(x_I)+V_{so}\frac{df(x_R)}{dr}\frac{\vec{L}\cdot\vec{S}}{r}$$

TABLE 9 - OPTICAL MODEL PARAMETERS USED IN THE DWBA CALCULATION.

	$^{10}B + {}^{3}He$	$^{12}N+n$
V(MeV)	173.	35.
r_o(fm)	1.07	1.25
a_R(fm)	0.82	0.65
r_c(fm)	1.4	1.25
W (MeV)	18.6	0.
r'_o(fm)	1.72	1.24
a'_I(fm)	0.76	0.65
W' (MeV)	0.	20.
V_{so}(MeV)	2.5	5.5

where the Coulomb potential $U_c(r)$ is given for a uniform charged sphere of radius $R = r_c A^{1/3}$. The function $f(x_i)$ has the expression

$$f(x_i) = 1+\exp\left(\frac{r-R_{oi}A^{1/3}}{a_i}\right)^{-1}$$

The factor describing the Thomas spin orbit term has been taken equal to 25 MeV in all calculations.

TABLE 10 - RESULTS OF THE DWBA AND CN ANALYSIS AND FIT PARAMETERS.

E_x (MeV)	J^π	J_T	Configurations	$E_{^3He}$ = 4.7.MeV		$E_{^3He}$ = 5.5 MeV	
				CD^2REL	F	CD^2REL	F
0	1^+	2	$1\,p_{3/2}{}^{+1}\,p_{1/2}$	1	0.239	1	0.121
0.977	2^+	2	$1\,p_{3/2}{}^{+1}\,p_{1/2}$	0.992	0.262	0.382	0.237
1.215	2^-	1	$1\,p_{3/2}{}^{+1}\,d_{5/2}$	0.677	0.061	0.355	0.207

For the two-proton transfer reactions the DWBA does not determine the spectroscopic factor and the calculated angular distributions are in arbitrary units. The parameters CD^2 and F are obtained from the experimental data best fit by means of the equations (1), then the resulting values of CD^2 have been normalized assuming $CD^2 = 1$ for the DWBA angular distribution of the ground state neutron group. On the contrary, the compound nucleus calculation results are in absolute values and the F coefficient arises directly from the comparison between the experimental differential cross sections and the calculated data, without any normalization. In Tab. 10 the values of these coefficients together with the level spin and parity hypothesis, the transferred total angular momenta and the adopted configurations are reported.

The comparison of the experimental differential cross sections with the calculated angular distributions for the neutron groups from the ground, first and second excited states of ^{12}N at energies $E_{^3He} = 4,7$ MeV and $E_{^3He} = 5,5$ MeV is reported in Fig. 8 and Fig. 9. The dashed dotted line and the dashed line represent the CN and DWBA

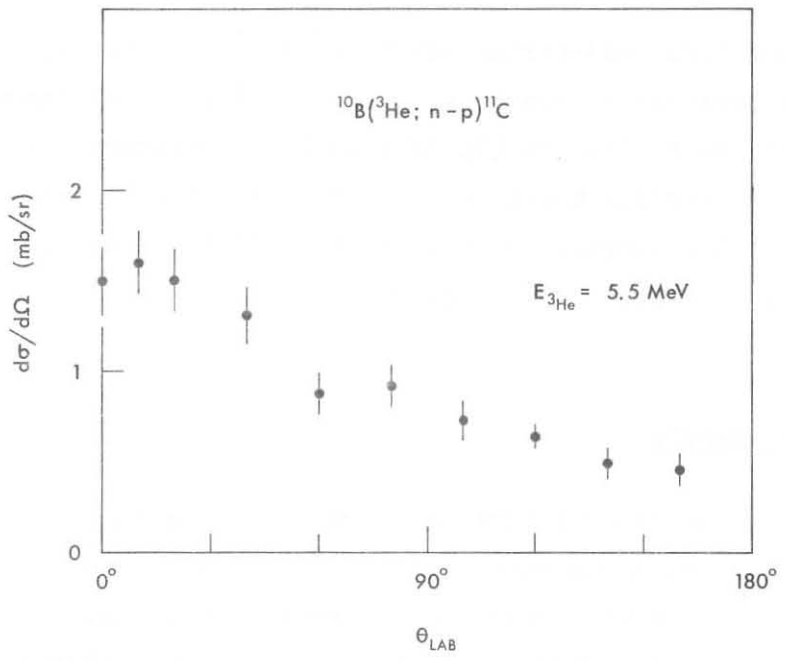

Fig. 15 - Neutron differential cross section for the $^{10}B(^3He;np)^{11}C$ reaction in the neutron energy range from 0,7 MeV to the maximum possible energy for different θ_{lab} at $E_{^3He} = 5,5$ MeV.

contributions respectively, and the solid line represents the sum of the two contributions.

1) The ground state of ^{12}N.

This state is reached starting from the ground state of the ^{10}B ($J^{\pi} = 3^{+}$). From the comparison of the calculated data with the experimental data the value $J_T = 2$ has been obtained for the transferred total angular momentum. This transfer is possible adding to the target nucleus an (1 p 3/2; 1 p 1/2) proton pair. The comparison of the measured quantities with those calculated assuming a non coherent sum of the $J_T = 2$ DWBA and the compound nucleus contributions with the transition sequence $3^{+} \rightarrow J^{\pi} \rightarrow 1^{+}$ is shown in Fig. 8.

2) The first excited level at $E_x = 977\ 14$ KeV.

This $J = 2^{+}$ level too is reached assuming an $J_T^{\pi} = 2$ transferred total angular momentum with a proton pair configuration (1p 3/2; 1p 1/2). The compound nucleus sequence is $3^{+} \rightarrow J^{\pi} \rightarrow 2^{+}$. The comparison of the calculated data with the experimental data is reported in Fig. 9.

3) The second excited level at $E_x = 1215 \pm 23$ KeV.

This is the first odd-parity level ($J^{\pi} = 2^{-}$) for the residual nucleus. It is possible to reach this level adding to the target nucleus a proton pair with the (1p 3/2; 1d 5/2) configuration. The transferred total angular momentum is $J_T = 1$, and the CN transition is $3^{+} \rightarrow J^{\pi} \rightarrow 2^{-}$. The comparison between the calculated and the experimental data is reported in Fig. 9.

7. - CONCLUDING REMARKS

By means of the neutron time-of-flight spectrometry the $^{10}B(^{3}He;n)^{12}N$ reaction has been studied at $E_{^3He} = 4{,}7$ MeV and $E_{^3He} = 5{,}5$ MeV. The neutron rows in the spectra obtained, at various angles between 0 and 160 degrees in the L.S. have been analyzed under the hypothesis that the $^{10}B(^{3}He; np)^{11}C$ reaction contributions are described from a constant matrix element for the mean energy distribution. The rows whose position and width at different angles

and energies obeyed the kinematic relations of the reaction have been assigned to the ^{12}N. In these conditions, as it results from the Fig. 16, the level scheme of ^{12}N undergoes a considerable increase of level number if compared to the data as yet reported in the literature. On the other hand the analysis of the spectra obtained with 4,6 meters of flight path, shows evident structures corresponding to the nuclear levels. Moreover the shape analysis of the spectra obtained by means of 2 meter flight path, even if insufficient in resolution, becomes worse whenever one of the other decay schemes reported in Fig. 16 is chosen. At this point it is indispensable to perform a high resolution measurement to obtain the maximum experimental separation (in the limits of the level widths) of the different rows resolved by means of a procedure of shape analysis in the present experiment.

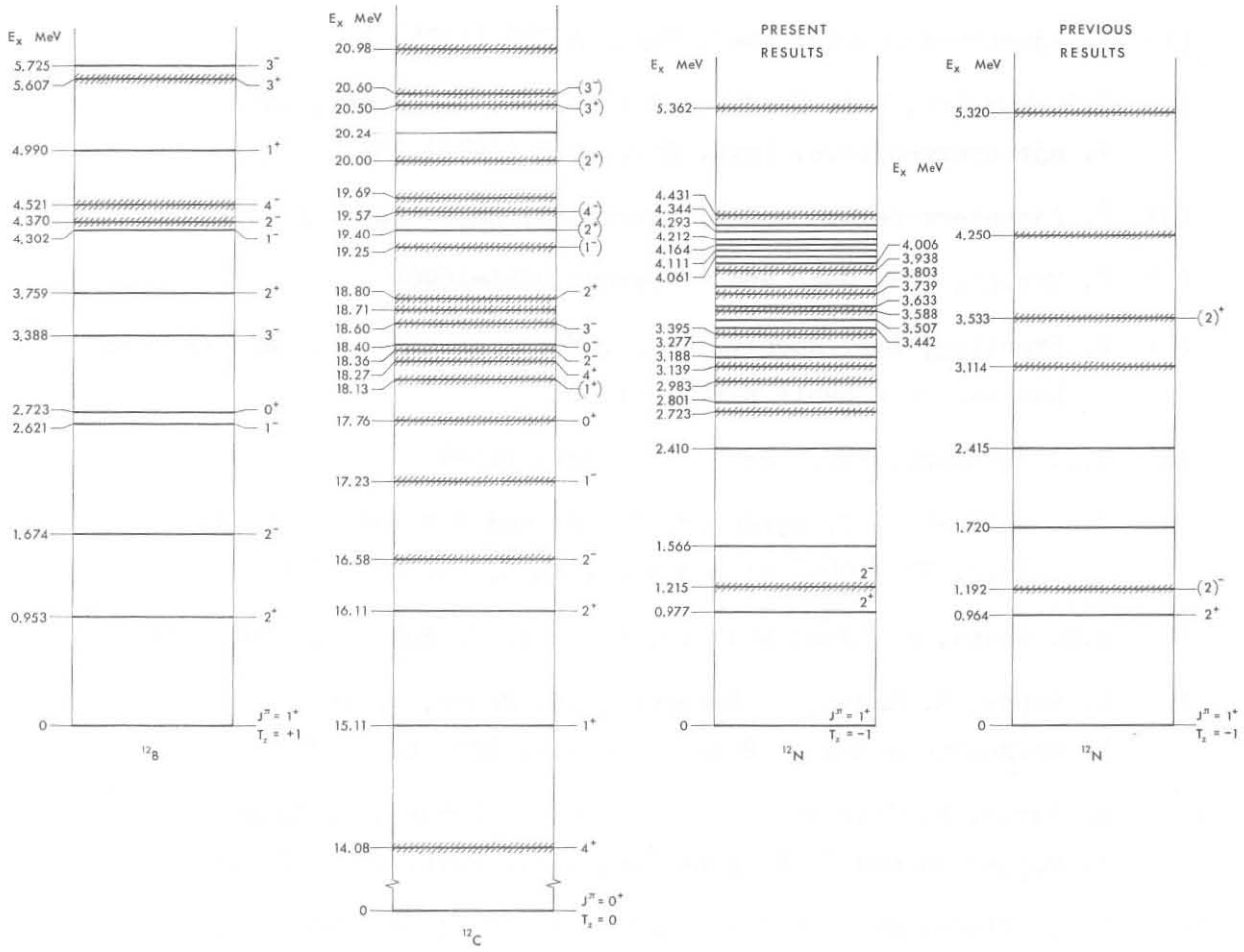

Fig. 16 - ^{3}He level diagram obtained in the present work up to E_x = 5,362 MeV compared with the diagrams of the ^{12}B and ^{12}C (1)(2) and the results on the ^{12}N reported in the work of Maguire et al.(2).

This report has been written to describe the results as yet obtained in the expectation of a nanosecond pulsed source availability for the high resolution measurements.

REFERENCES

(1) F. Ajzenberg-Selove: Nucl. Phys. A 248 (1975) 1

(2) C.F. Maguire, D.L. Hendrie, D.K. Scott, J. Maboney and F. Ajzenberg-Selove: Phys. Rev.. C13 (1976) 933

(3) F. Ajzenberg-Selove and T. Lauritsen: Nucl. Phys. A114 (1968) 1

(4) C. Maples, G.W. Goth and J. Cerny: UCRL-16964

(5) F. Everling, L.A. Koenig, J.H.E. Mattauch and A.H. Wapstra USAEC Nuclear data table part I (1960)

(6) R.W. Kavanagh: Phys. Rev. 133 (1964) B1504

(7) C.D. Zafiratos, F. Ajzenberg-Selove and F.S. Dietrich: Nucl. Phys. 77 (1966) 81 and Nucl. Phys. 89(1966) 706.

(8) J.M. Adams, A. Adams and J.M. Calvert, J. Phys. A1 (1968) 549.

(9) W. Bohne, M. Hagen, H. Homeyer, K.H. Mayer, H. Lettau, H. Morgenstern and J. Scheer, Physic. Rev. C2 (1970) 2072

(10) H. Fuchs, K. Grabisch, D. Hilscher, U. Jahnke, H. Kluge, T. Masterson and H. Morgenstern, Nucl. Phys. A234 (1974) 61

(11) G.G. Ohlsen: Nuclear Inst. and Meth. 37 (1965) 240

(12) P.D. Kunz, University of Colorado, unpublished

(13) E. Sheldon and R.M. Strang, Comp. Phys. Comm. 1 (1969) 35